EXPERIMENTAL AND THERMODYNAMIC ANALYSIS OF A BOTTOMING ORGANIC RANKINE CYCLE (ORC) OF GASOLINE ENGINE USING SWASH-PLATE EXPANDER

J. Galindo, S. Ruiz, V. Dolz[1], L. Royo-Pascual

CMT – Motores Térmicos, Universitat Politècnica de València, Spain

R. Haller, B. Nicolas, Y. Glavatskaya

Valeo Systèmes Thermiques, France

Abstract

This paper deals with the experimental testing of an Organic Rankine Cycle (ORC) integrate in a 2 liter turbocharged gasoline engine using ethanol as working fluid. The main components of the cycle are a boiler, a condenser, a pump and a swash-plate expander. Five engine operating points have been tested, they correspond to a nominal heat input into the boiler of 5, 12, 20, 25 and 30 kW. With the available bill of material based on prototypes, power balances and cycles efficiencies were estimated, obtaining a maximum improvement in the ICE mechanical power and an expander shaft power of 3.7% and 1.83 kW respectively. A total of 28 steady-state operating points were measured to evaluate performance of the swash-plate expander prototype. Operating parameters of the expander, such as expander speed and expansion ratio, were shifted. The objective of the tests is to master the system and understand physical parameters influence. The importance of each parameter was analyzed by fixing

[1] V. Dolz. CMT-Motores Térmicos, Universitat Politècnica de Valencia, Camino de Vera s/n, 46022 Valencia, Spain. Phone: +34 963877650 Fax: +34 963877659 e-mail: vidolrui@mot.upv.es

all the parameters, changing each time one specific value. In these sensitivity studies, maximum ideal and real Rankine efficiency value of 19% and 6% were obtained respectively.

Keywords

Organic Rankine Cycle, Gasoline engine, Waste Heat Recovery, Swash-plate expander, ethanol

NOMENCLATURE

Acronyms

CFC	Chlorofluorocarbon
CMT	Centro de Motores Térmicos
EGR	Exhaust Gas Recirculation
GHG	Green House Gases
HCFC	Hydrochlorofluorocarbon
HDV	Heavy Duty Vehicle
HFC	Hydrofluorocarbons
ICE	Internal Combustion Engines
LDV	Light Duty Vehicle
MDV	Medium Duty Vehicle
NFPA	National Fire Protection Association
ORC	Organic Rankine Cycle
TEG	Thermoelectric generator
WHR	Waste Heat Recovery
NEDC	New European Driving Cycle

Notation

Latin

Cp	Specific heat at constant pressure	kJ/kgK
Cv	Specific heat at constant volume	kJ/kgK
D	Total displacement of the expander	m^3
$\dot{m}$	Mass flow	kg/s
h	Specific enthalpy	kJ/kg
T	Temperature	°C
I_l	Current	A
N	Speed	rpm
P	Power	kW
Pe	Electric power	kW
Q_{fuel}	Total fuel power	kW
U_l	Voltage	V
X	Mass fraction	

Greek letters

τ_e	Expander torque	Nm
ρ	Density	kg/m^3
$cos\varphi$	Power factor	-
η	Efficiency	

Subscripts

$Boil$	Boiler
EG	Exhaust gases side
ET	Ethanol side
in	Inlet conditions
out	Outlet conditions
Exp	Expander
$Cond$	Condenser
iso	Isentropic conditions
W	Water side
$Pump$	Pump
m	Average
GE	Gasoline engine
$ORC-GE$	Organic Rankine Cycle-Gasoline engine
mec	Mechanical
$Carnot$	Carnot
l	Lower temperature level in the cycle
u	Higher temperature level in the cycle
$Rankine_{ideal}$	Ideal Rankine
$Rankine_{real}$	Real Rankine
vol	Volumetric
$Gasoline$	Gasoline side
Air	Air

1. Introduction

Transportation accounts for approximately 25% of world energy demand (61.5% of all the used oil each year), so that, an improvement in efficiency could lead to an important saving in the amount of energy consumed [1]. Despite global alerts regarding to the use of fossil fuels, it can be said that global energy demand in following years is projected to be 50-60% more than current levels [2], thus energy efficiency and vehicle performance improvements will play an essential role in reducing GHG emissions.

Internal combustion engines transform chemical energy into mechanical energy through combustion; however, only about 15-32% of this energy is effectively used to produce work [3], while most of the fuel energy is wasted through exhaust gases and coolant.

Upcoming CO_2 regulations will lead to introduce different technologies, increasing the overall efficiency of the whole powertrain without raising GHG emissions. While some hybrid systems, such as start-stop and regenerative breaking system, try to optimize the vehicle when it is stopped and slowed down respectively, it will not be enough to reach future CO_2 demands, especially when the engine is loaded. Thus, waste heat recovery technologies seem to assume an essential role in the new regulations of the forthcoming decade [4], [5]. Since the invention of ICE, there have been some attempts to increase the effective power using Waste Heat Recovery sources (Coolant and Exhaust Gases). The market for Waste Heat Recovery will grow up moderately by heat-to-heat exchanger and TEG. Furthermore, turbo-compounding and Rankine cycles will be focused in MD/HD commercial vehicles[6].

In the present study, a swash-plate expander is tested in an Organic Rankine Cycle test bench coupled to a turbocharged gasoline engine and using ethanol as working fluid.

Although several simulations and theoretical papers about ORC in IC engines exist [7]–[9], few experiments have been developed with a volumetric expander which could generate energy. Table 1 shows a summary of the main experimental setups using ORC to recover waste heat energy. Several tests have been done using turbines and expanders. Most of them corresponds to scroll expanders [10]–[13] and rotary vane ones [14]–[17]. Reciprocating machines are considered by Glavatskaya et al. [18] as the most promising technology for a waste heat recovery applications. Between reciprocating expanders, swash-plate expanders are increasingly taking into account due to its versatility, compactness, robustness and a good specific power. This type of expanders are preferred because they are suitable for higher pressure ratios comparing to scroll and rotary vane expanders. These higher pressure ratios imply a better efficiency of the global ORC.

Table 1. Summary of main experimental tests in ORC cycles

Expander type	Researcher	Application	Working fluid	Power source (kW)	Power expander (kW)
Turbine	Chammas [3]	SI engine SI engine SI engine	Water R245fa Isopentane	50-200 50-200 50-200	6.028 6.664 6.634
	Yagoub [19]	Hybrid solar-gas driven system	n-pentane HFE-301	25 25	1.5 1.5
	Yamamoto [20]	Electric heaters	Water R123	19.9 13	0.15 0.15
	Seher [21]	Electrical hot gas generators	Water	250	9
Scroll	Kim [22]	Gas tank generator	Water	-	11
	Peterson [23]	Circulating hot oil loop	R123	3.54	0.256
	Manolakos [24]	ORC system coupled to a RO desalination unit	R134a	35	0.891
	Declaye [10]	Combined Heat and Power Cycle	R245fa	20	1.8
	Lemort [25]	Gas cycle	R245fa	-	2
Piston expander	Bracco [26]	Electrical hot gas generators	R245fa	-	1.3
Swash-plate expander	Endo [27]	SI engine	Water	84	4

Volumetric expanders are characterized by a built-in volume ratio, which corresponds to the volumetric expansion of an internal pocket. In this pocket, the working fluid will expand producing effective work that could be harnessed to improve ICE mechanical efficiency [28]. The volumetric expansion ratio, which is defined as the ratio of the discharge volume to the swept volume, should fit into the actual working fluid expansion ratio in order to avoid under-expansion and over-expansion losses [29]. In systems for recovering waste heat from vehicle exhausts, the available waste heat depends on the gas temperature and the exhaust mass flow. Thus, in order to maintain the higher efficiencies in all the

engine operating conditions a variable expansion mechanism is required to adjust the expansion ratio of the expander to the optimal expansion ratio of the working fluid. Displacement expanders run at lower rotational speeds, which involve less cost-intensive technologies than turbo expanders [30]. Lower flow rates and higher expansion ratios could be reached, making displacement expanders the main technology for recovering waste heat from low temperature sources and low expander power in vehicle applications.

The first design option in the ORC has been the selection of the waste heat sources. These sources are located in the main flows of lost energies in IC engines, the cooling loop and the exhaust gases [31]. Duparchy et al. [32] indicates that the exhaust gases represents the greater recovery potential due to large difference in the thermodynamic properties of the two fluids and lower mass flow rates comparing exhaust gases with water (cooling loop), thus, irreversibility is reduced. Teng et al. [33] showed that EGR and exhaust gases are the most suitable sources in terms of energy recovery because of its exergy value. V. Macián et. al [34] recommends the contribution of EGR, exhaust gases and aftercooler in order to simplify the bottoming cycle structure. V. Dolz et. al [35] studied different configurations of waste heat sources and concluded that the configuration with high temperature heat sources (EGR, exhaust gases and aftercooler) is the most suitable one in order to reduce system complexity and cost.

The second design option has been the selection of the working fluid. Trying to optimize the cycle, both in thermodynamic and economic aspects, different working fluids are have been used in automotive applications: Water and ethanol were used by Freeman et. al in a dual-circuit system from BMW [36], water were

used by Endo [27] in an 2 l Honda, ethanol were used by Teng et. al [37] and R245fa by Boretti [38]. Water is a very convenient fluid because its low cost and high availability, non-toxicity, non-flammability, environmentally friendly, chemical stability and low viscosity [39]. However, it is not the ideal working fluid in terms of recovering low heat sources, particularly heat of exhaust gases in ICEs, due to the high operating boiling pressures, low condensing pressures, high heat of vaporization and high triple-point temperature [3]. For this reason, using water as the working fluid will result in larger systems, increasing weight and cost of the global vehicle [3]. Synthetic HFC refrigerants, among which R245fa is highlighted, have been identified as suitable candidates for recovering moderate to low temperature waste energy [40]–[48]. However, its GWP is higher than natural organic working fluids, so its use is being phasing down. Zeotropic mixtures have been considered by Zhan et al. [49] in order to reduce irreversibilities in the heat exchangers. Among organic fluids, several authors consider ethanol as a promising fluid due to its great features in energy recovery aspect in the temperature range of a vehicle application (450ºC-100ºC). Ethanol has been taken into account for its environmental, thermo-physical properties (high expansion ratios, condensation temperatures at atmospheric pressure and low freezing point) and cost features. Although ethanol is positively evaluated taking into account previous characteristics, it has been classified as serious hazard by NFPA due to its high flammability. Seher et. al [21] concluded that ethanol is one of the most favorable solution using a piston machine. Gibble et. al [50] selected ethanol as the best working fluid for a successful ORC for a HD truck.

Despite of these theoretical studies, where the ethanol has proven to be the most suitable working fluid for this type of installations, experimental works of this fluid in ORC have not been published. Such experimental facilities with ethanol use a flammable working fluid. Therefore, it is necessary to take the necessary safety measures to prevent accidents arising from the use of this fluid.

Thus, the objective of this paper is to evaluate the impact of adding an ORC cycle on ICE by means of tests realized in our lab using a swash-plate expander and ethanol as working fluid. The partial objectives of this paper are:

- To characterize the experimental setup (Section 2).
- To estimate the amount of energy obtained of this system and compare cycle performances (Section 3 and 4).
- To determine the main parameters affecting cycle efficiencies by means of sensitivity analysis (Section 5).

2. Experimental setup

2.1. Description of the gasoline engine

The gasoline engine used in these tests is an inline four-cylinder turbocharged engine with a volumetric capacity of 2 liter. The maximum engine torque is 308 Nm at 3000 rpm and 100% load. The maximum engine power is 153 kW at 5500 rpm and 100% load. The engine is situated in a test bench and is instrumented to measure torque, speed, temperature in the exhaust line (before and after the catalyzer), injected mass of fuel and mass flow in the intake line. The exhaust gas power in each engine operating point is calculated from the temperature measurements and the exhaust mass flow estimation, from the measurements of intake air mass flow and injected fuel. The ambient conditions are considered as

the reference state. It is represented in Fig. 1. The Kriging interpolation method was used to plot the contour lines of Fig. 1. It shows that the available exhaust gas energy increases with engine speed and engine load. The highest point corresponds to 5500 rpm and full load, with a value of 153 kW, whereas the lowest point corresponds to 1000 rpm where the engine generates almost any waste heat. Additional blue lines plotted in Fig. 1 indicate the ratio of the exhaust gases power to the total fuel power obtained from the calorific value of the injected fuel. It shows that although the greater exhaust gas power is reached at high engine speed and torque, the biggest recovery potential from the input fuel power is obtained at medium torque and engine speeds. At low engine speed heat losses to the ambient are magnified, also for high engine speed mechanical losses are increased. Therefore, the power available in exhaust gases is maximized at medium speed and torque operating points.

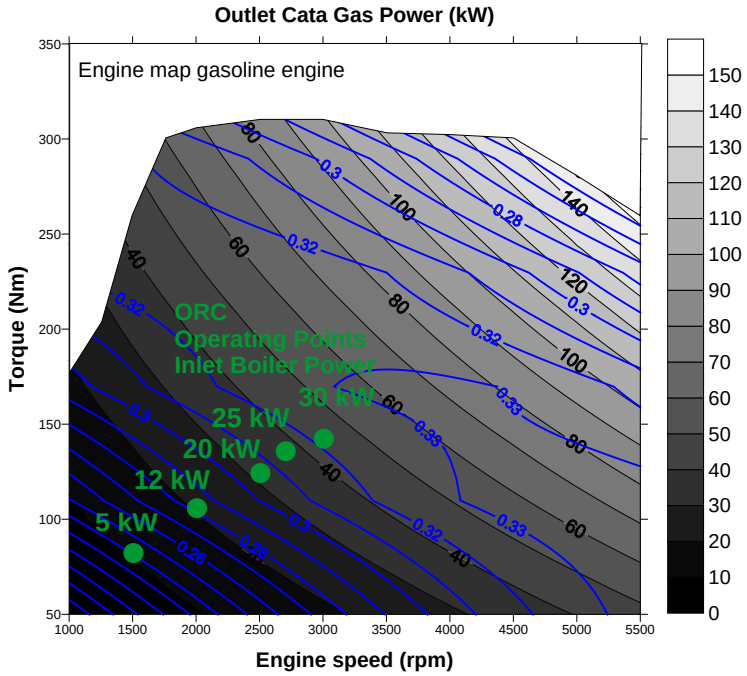

Fig. 1. Exhaust gases power and percentage of exhaust gases power to the input fuel power in the engine

Five operating points, listed in Table 2 and plotted in Fig. 1, have been chosen for design and simulations. The most frequently engine operating points depend on the size of the engine and the passenger driving mode. Fig. 2 shows the Ford Explorer NEDC cycle and the points tested in the ORC. As shown in this figure, points 1, 2 and 3, which corresponds to a boiler power of 5, 12 and 20 kW respectively are normal engine operating points, thus it is justified its measurement. NEDC cycle is characterized by soft acceleration and gradient of 0%. These Waste Heat Recovery systems improve their efficiencies when the heat source power increases. Therefore, two points (4 and 5), which corresponds with normal engine operating points in highways, have been added, in order to estimate maximum WHR system efficiencies. They will be essential to evaluate the viability of the system.

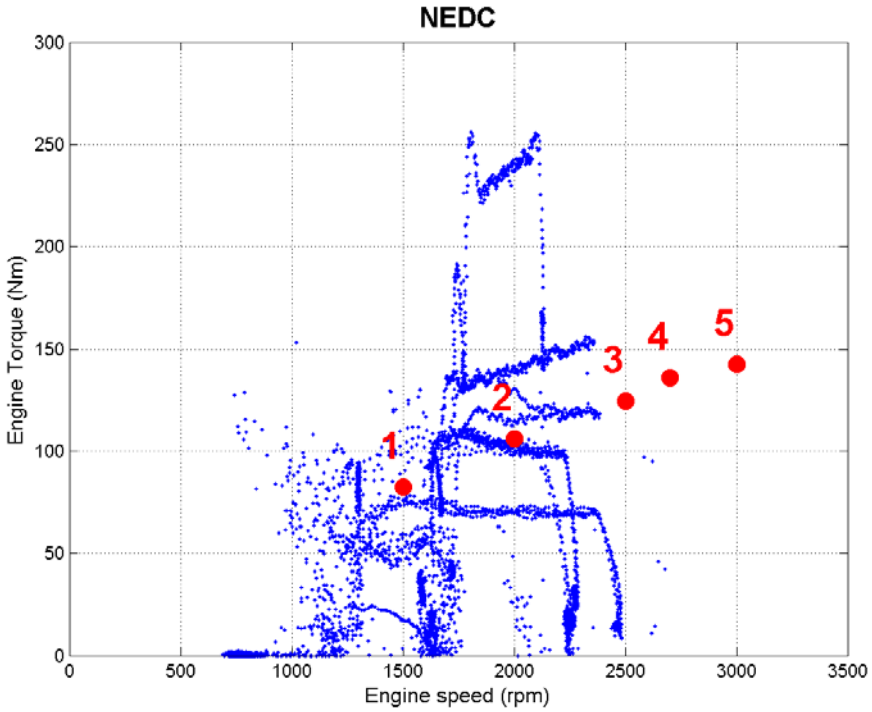

Fig. 2. NEDC and engine operating points

Under these five conditions, the temperatures of the exhaust gases are within 429-673 °C and the mass flow of exhaust gases varies from 15 to 48 g/s. These points belong to five vehicle operating points of Ford Explorer 2.0 EcoBoost gasoline direct injection engine at steady state simulation conditions. Every engine operating point has an equivalent boiler power of 5, 12, 20, 25 and 30 kW and throughout the whole paper references to them will be made. Differences between outlet catalyzer gas power and inlet boiler power are produced by heat losses in the exhaust line.

Table 2. Engine operating points chosen for design and simulations bottoming cycle

	Op. point 1	**Op. point 2**	**Op. point 3**	**Op. point 4**	**Op. point 5**
Vehicle speed (km/h)	63	84	106	114	126
Gear demanded	5	5	5	5	5
Gradient	0.6%	0.9%	0.8%	0.9%	0.7%
Engine speed (rpm)	1500	2000	2500	2700	3000
Engine torque (Nm)	82.4	106.0	124.5	136.0	142.6
Fuel power (kW)	40.5	69.6	100.5	119.1	140.8
Engine power output (kW)	12.9	22.2	32.5	38.5	44.8
Inlet temperature of the exhaust gas (°C)	429	526	602	646	673
Mass flow exhaust gas (g/s)	15	24	35	41	48
Exhaust gases Power (kW)	5	12	20	25	30

Fig. 3 shows the measured exhaust gas temperature at the boiler inlet with exhaust gas mass flow for previous five engine operating points. It should be noticed that these points correspond to low operating points in the engine map. Temperature is measured after the catalytic converter.

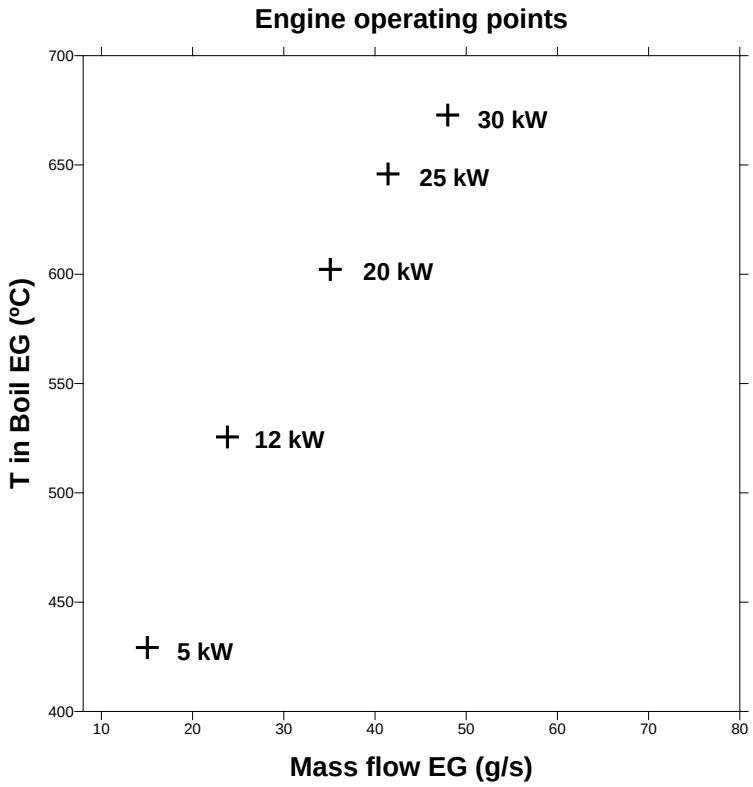

Fig. 3. Measured exhaust gas temperature at the boiler inlet with exhaust gas mass flow

2.2. Description of the ORC mock-up

In this section, a brief description of the ORC system is given, explaining the main characteristics of the ORC. Fig. 4 shows a photo for the experimental set up of the ORC system used in this study.

Fig. 4. Experimental ORC installation

Fig. 5 shows the schematic diagram of the ORC cycle. It operates as follows: Engine exhaust gases pass through the boiler and then they exchange heat into the ethanol. Ethanol is pumped into the high pressure loop and sequentially it is evaporated in the boiler and slightly superheated. Then, the vapor flows into the expander where enthalpy is transformed into effective work measured by a torque measuring unit. Low pressure vapor is extracted from the expander and flows to the condenser, where it condenses using cooling water. The pump is a stainless steel direct drive plunger pump supplied by CAT PUMPS. It is connected to an electrical motor with a maximum speed of 1725 rpm. At this speed, the pump delivers 7 l/min. The boiler ensures the heat transfer from exhaust gas to working fluid. It is based on plate and fin technology and it was specifically designed and supplied by Valeo Systèmes Thermiques. The condenser and the subcooler are plate and fin heat exchangers chosen among industrial residential products. The condenser is followed by an expander vessel in order to impose the low pressure

in the installation and a liquid reservoir. The expander prototype is a piston swash-plate. Few installations have been tested with this type of expanders [27]. Additional sensors, such as, temperature and pressure sensors have been placed at the inlet and the outlet of the different elements, several mass flow sensors have also been installed to measure the mass flow of different fluids.

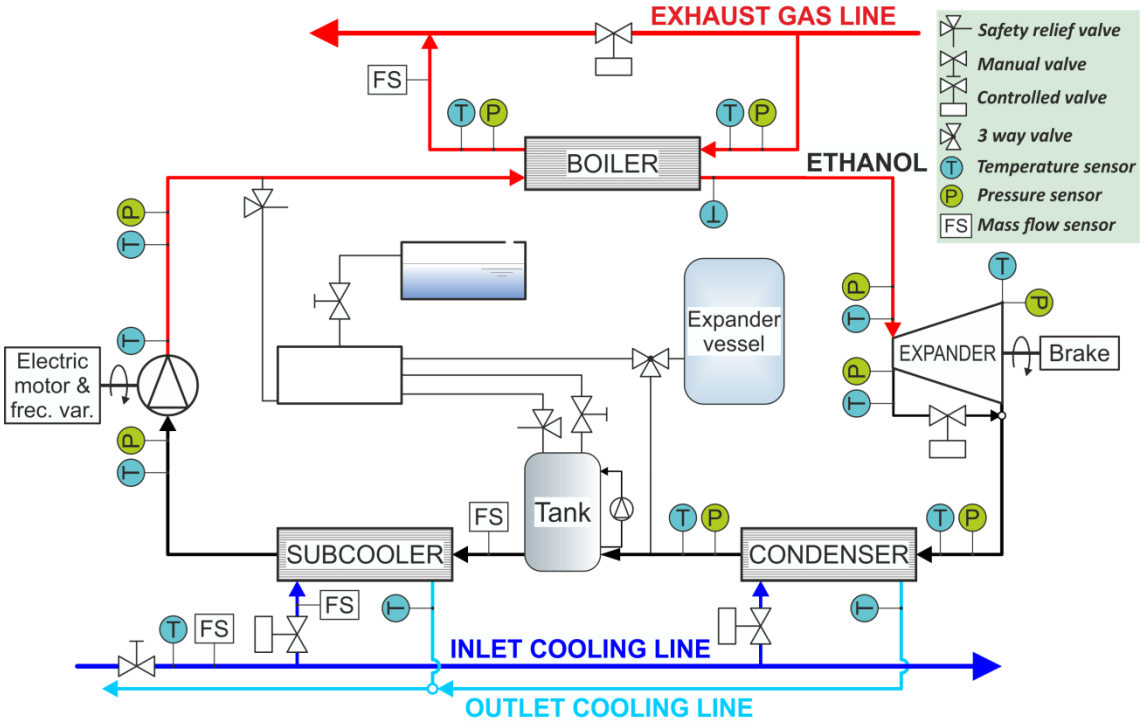

Fig. 5. Schematic diagram of the bottoming cycle

Measurements of temperatures in the ORC cycle were made through 14 K-type thermocouples with an accuracy of $\pm\ 2.5°C$ installed in each element of the cycle (boiler, condenser, pump and expander) at the inlet and outlet. Piezoresistive pressure sensors made by Kistler were used at the inlet and the outlet of the main elements of the installation. Three types of pressure sensors were installed, depending on the pressure range measured. The high pressure flow (from the outlet of the pump and the inlet of the expander) was measured using the pressure sensor Kistler type 4260A750B7BD00Y1. The medium pressure flow (from the outlet of the expander to the inlet of the pump) was measured by

different Kistler type 4260A075B7BD00Y1 sensor. The pressure drop through the boiler on the exhaust side was measured using a Kistler type 4260A030B7BD00Y1. This type of sensor has an accuracy of $\pm 0.05\%$ in full scale range, which is 50, 5 and 2 bar respectively. Regarding mass flow sensors, water was measured by an electromagnetic flow sensor made by ADMAG AE (AE 202 mg) with an accuracy of $\pm 0.5\%$ FS. The flow rate of the working fluid was measured using a Coriolis measurement unit made by Emerson with an accuracy that varies from $\pm 0.273\%$ to $\pm 1.001\%$ depending on the measured value. Torque and expander speed were measured in order to compute the power delivered by the expander. The Torque measuring unit used was 4550A200S10N1KA0 model made by Kistler. Its accuracy is 0.05% in full scale (200 Nm). Range and accuracy of sensors are summarized in Table 3.

Table 3. Range and accuracy of sensors

	Measurement principle	Range	Accuracy
Exhaust gas pressure	Piezoresistive	0-2 bar	0.05% FS
Ethanol high pressure loop	Piezoresistive	0-50 bar	0.05% FS
Ethanol low pressure loop	Piezoresistive	0-5 bar	0.05% FS
Temperatures	K-type thermocouples (class 2)	(-270)-(1,372)K	±2.5°C
Ethanol flow meter	Coriolis flow meter	0-2,720 kg/h	±0.1%
Water flow meter	Electromagnetic flow sensor	0.3-1 m/s	±0.5% of rate
Expander rotational speed	Optical tachymeter	0-20,000 rpm	±1 rpm
Expander torque meter	Strain gauges	0-200 Nm	0.05%FS

A total of 28 steady-state points have been tested varying several parameters to evaluate cycle and expander efficiencies under a wide range of conditions. The global analysis of these points is presented in the sensitivity analysis, however, in order to evaluate the potential of this ORC only five operating points have been chosen for design and simulations. These points, listed in Table 4, correspond to optimum points tested for each boiler power (5, 12, 20, 25 and 30 kW).

Table 4. ORC operating points chosen for design and simulations bottoming cycle

	Op. point 1	Op. point 2	Op. point 3	Op. point 4	Op. point 5
High pressure (bar)	14.8	15.7	18.7	24.0	24.8
Low pressure (bar)	2.3	1.9	2.0	2.5	2.5
Expansion ratio	6.4	8.3	9.2	9.4	9.5
Mass flow (kg/h)	16.67	39.95	64.95	82.01	102.87
Pump speed (rpm)	69	154	250	313	403
Expander speed (rpm)	1018	2527	3511	3021	3354
Expander torque (Nm)	2	2.7	3.5	5	5.2
Expander power (kW)	0.21	0.71	1.28	1.58	1.83
Boiler power (kW)	5	12	20	25	30

In these tests, the system has been controlled commanding three parameters: the speed of the pump, in order to control the mass flow of ethanol flowing through the installation, the balloon pressure of the expander vessel, in order to control the outlet pressure of the expander, and the expander speed, in order to control the high pressure at the inlet of the expander.

3. Energy balances in the cycle

Temperatures and pressures were measured at the inlet and outlet of the main elements of the system (boiler, expander, condenser and pump). Moreover, mass flow rates have been measured both in the ethanol, water and exhaust gases. Therefore, all the elements are considered as black boxes with inlet power and

outlet powers estimated using the equations 1-14. Differences between inlet powers and outlet useful powers are the power losses of the different elements.

3.1. Boiler

The inlet power of the boiler is calculated using inlet and outlet measurements of exhaust gases temperatures and considering them as ideal gases, Eq. 1:

$$P_{Boil\_EG} = \dot{m}_{EG} * \left(h_{in\_Boil\_EG} - h_{out\_Boil\_EG}\right) = \dot{m}_{EG} * Cp_{EGt} * \left(T_{in\_Boil\_EG} - T_{out\_Boil\_EG}\right) \quad (1)$$

where Cp_{EGt} is the global specific heat at constant pressure for exhaust gases, $\dot{m}_{EG}$ is the exhaust gas mass flow through the installation, $T_{in\_Boil\_EG}$ and $T_{out\_Boil\_EG}$ are respectively the inlet and outlet exhaust gas temperature of the boiler in the exhaust gas side. Cp_{EGt} has been estimated considering the properties of the mixture (lean or rich) and Mayer's equation for ideal gases [51]. Depending on the ratio between fuel and air of each particular point a different equation is used, using Eq. 2 when the mixture is rich and Eq. 3 when the mixture is lean. Eq. 4 and 5 shows the correlation obtained for the specific heat at constant volume using the same methodology as Lapuerta [52] did for Diesel, but in this case for gasoline.

$$Cp_{EGt} = X_{gasoline} * Cp_{gasoline} + X_{EG} * Cp_{EG} \quad for\ rich\ mixture \quad (2)$$

$$Cp_{EGt} = X_{air} * Cp_{air} + X_{EG} * Cp_{EG} \quad for\ lean\ mixture \quad (3)$$

$$Cp_{EG} = R + Cv_{EG} = \\ = \mathrm{R} + (655.1103865 + 0.401687993 * \mathrm{T} - 0.0000698091 \\ * T^2 - 0.00000000931055 * T^3 + 2.53355\mathrm{E} - 12 * T^4) \quad (4)$$

$$Cp_{gasoline} = R + Cv_{gasoline} = \\ = R + (-12291002.2 * T^{-2} + 227580.041 * T^{-1} \\ - 1545.51269 + 10.8382363 * \mathrm{T} - 0.00837844 * T^{2} \\ + 0.0000032557 * T^{3} - 0.00000000040429 * T^{4} \\ - 72.78128689) \quad (5)$$

$$Cp_{air} = 0{,}000226527253919308 * \mathrm{T} + 0{,}977898191692365 \quad (6)$$

where Cp_{EG} , $Cp_{gasoline}$, Cp_{air} is the specific heat at constant pressure for exhaust gases, gasoline and air respectively. $X_{gasoline}$ is the fraction of additional gasoline respect to the stoichiometric mixture divided by the sum of fuel and air. X_{air} is the fraction of additional air respect to the stoichiometric mixture divided by the sum of fuel and air. X_{EG} is the remainder fraction of exhaust gases divided by the sum of fuel and air. Cv_{EG} is the specific heat at constant volume for exhaust gases. $Cv_{gasoline}$ is the specific heat at constant volume for gasoline. Cp_{air} is the specific heat at constant pressure for air and T is the temperature of exhaust gases. Cp_{EG} and $Cp_{gasoline}$ have been obtained using Mayer equation for ideal gases using Eq. 4 and Eq. 5. Cp_{air} were calculated by REFPROP 7 [53] develop by the National Institute of Standards and Technology of the United States. These correlations have been calculated using an average between inlet and outlet temperature.

The outlet power of the boiler is calculated using inlet and outlet temperature and pressure measurements of ethanol in the boiler, Eq. 7.

$$P_{Boil\_ET} = \dot{m}_{ET} * \left(h_{in\_Boil\_ET} - h_{out\_Boil\_ET}\right) \quad (7)$$

Where $h_{in\_Boil\_ET}$ and $h_{out\_Boil\_ET}$ can be obtained using temperature and pressure at the inlet and outlet of the boiler. The properties of ethanol are calculated by REFPROP 7 [53] develop by the National Institute of Standards and Technology of the United States.

3.2. Expander

The expansion power can be calculated based on Eqs. 8, 9 and 10, which corresponds to isentropic power, expansion power and shaft power respectively.

$$P_{Exp\_isentropic} = \dot{m}_{ET} * \left(h_{in\_Exp\_ET} - h_{out\_Exp\_ET\_iso}\right) \quad (8)$$

$$P_{Exp\_expansion} = \dot{m}_{ET} * \left(h_{in\_Exp\_ET} - h_{out\_Exp\_ET}\right) \quad (9)$$

$$P_{Exp\_shaft} = \tau_{exp} * N_{exp} \quad (10)$$

Where $h_{in\_Exp\_ET}$ and $h_{out\_Exp\_ET}$ have been calculated using temperature and pressures at the inlet and outlet of the expander. In Eq. 8, $h_{out\_Exp\_ET\_iso}$ is the isentropic enthalpy at the outlet of the expander, calculated from an isentropic expansion between the temperature and pressure inlet conditions and the pressure at the outlet of the expander. As regards shaft power, τ_{exp} is the expander torque and N_{exp} is the expander speed. In order to lubricate the expander, a small quantity of oil has been added to the working fluid. It has been considered in the calculations, taking into account the percentage of oil and estimating its calorific capacity using its data sheet.

3.3. Condenser

The outlet power of the condenser is calculated using inlet and outlet conditions of water in the condenser, considering them as an incompressible fluid, Eq. 11:

$$P_{Cond\_W} = \dot{m}_W * \left(h_{in\_Cond\_W} - h_{out\_Cond\_W}\right) = \dot{m}_W * C_{p_W} * \left(T_{in\_Cond\_W} - T_{out\_Cond\_W}\right) \quad (11)$$

Where Cp_W is the specific heat at constant pressure for water, $\dot{m}_W$ is the water mass flow through the installation, $T_{in\_Cond\_W}$ and $T_{out\_Cond\_W}$ are respectively the inlet and outlet exhaust water temperature of the boiler in the condenser. Cp_W has been considerate 4.18 kJ/kgK for water.

The inlet power of the condenser is calculated using inlet and outlet temperatures and pressures of ethanol in the condenser, Eq. 12.

$$P_{Cond\_ET} = \dot{m}_{ET} * \left(h_{in\_Cond\_ET} - h_{out\_Cond\_ET}\right) \quad (12)$$

Where $h_{in\_Cond\_ET}$ and $h_{out\_Cond\_ET}$ can be obtained using temperature and pressures at the inlet and outlet of the condenser.

3.4. Pump

The outlet power of the pump is calculated using inlet and outlet temperatures and pressures of ethanol in the pump. It is calculated using Eq. 13. The assumption of incompressible fluid is imposed.

$$P_{Pump\_ET} = \dot{m}_{ET} * \left(h_{out\_Pump\_ET} - h_{in\_Pump\_ET}\right) = \dot{m}_{ET} * \frac{1}{\rho_m} * \left(P_{out\_Pump\_ET} - P_{in\_Pump\_ET}\right) \quad (13)$$

Where ρ_m is the average density considering inlet and outlet conditions, $P_{in\_Pump\_ET}$ is the pressure at the inlet of the pump and $P_{out\_Pump\_ET}$ is the pressure at the outlet of the pump.

The inlet electric power needed by the pump can be calculated by Eq. 14.

$$Pe_{Pump\_ET} = \sqrt{3} * U_l * I_l * cos\varphi \quad (14)$$

Where U_l is the line voltage and I_l is the line current of the three-phase pump. In this particular case U_l corresponds to 400V and $cos\varphi$ corresponds to 0.57.

3.5. Experimental results (energy balances)

Eqs. 1-14 have been applied to calculate the power balances in the main components of the system: Boiler, condenser, swash-plate expander and pump. Table 5 shows the power balances in all the elements of the installation. The reduction of the engine load (from operating point 5 to 1) results in a decrease in the temperature and mass flow of the exhaust gases and, thus, the heat absorbed in the boiler, as shown the 1st and 2nd columns of Table 5. As expected, the greater power in the boiler is absorbed, the greater amount of energy in the shaft of the expander is produced, as shown in columns 5th, 6th and 7th of Table 5. Regarding the ratio of P_{boiler}ET and P_{boiler}EG, it varies from 93% to 98% depending on the operating point.

Table 5. Power balances in the system

Op. point (kW)	P_{boiler} EG (kW)	P_{boiler} ET (kW)	P_{cond} ET (kW)	P_{cond} W (kW)	$P_{expander}$ iso (kW)	$P_{expander}$ expansion (kW)	$P_{expander}$ shaft (kW)	P_{pump} ET (kW)	Electric Power pump (kW)
5	5.36	5.03	4.2	4.7	0.74	0.64	0.21	0.007	0.063
12	12.07	11.72	10.31	9.91	1.93	1.18	0.71	0.020	0.102
20	19.45	18.86	16.86	16.39	3.2	1.70	1.28	0.039	0.118
25	24.22	23.35	20.95	21.03	4.14	2.1	1.58	0.045	0.157
30	29.51	28.95	26.16	25.21	5.18	2.47	1.83	0.085	0.195

As shown also in Fig. 6, the expansion power produced by the expander increases as the power absorbed by the boiler is magnified. It should be noted that the difference between boiler power and cooling water power does not remain constant, increasing with the power of the boiler. On the other hand, power in the pump could be neglected. It can be concluded from Fig. 6 that the maximum expansion power is achieved under 30 kW (Operating point number 5) obtaining an expander power of 1.83 kW.

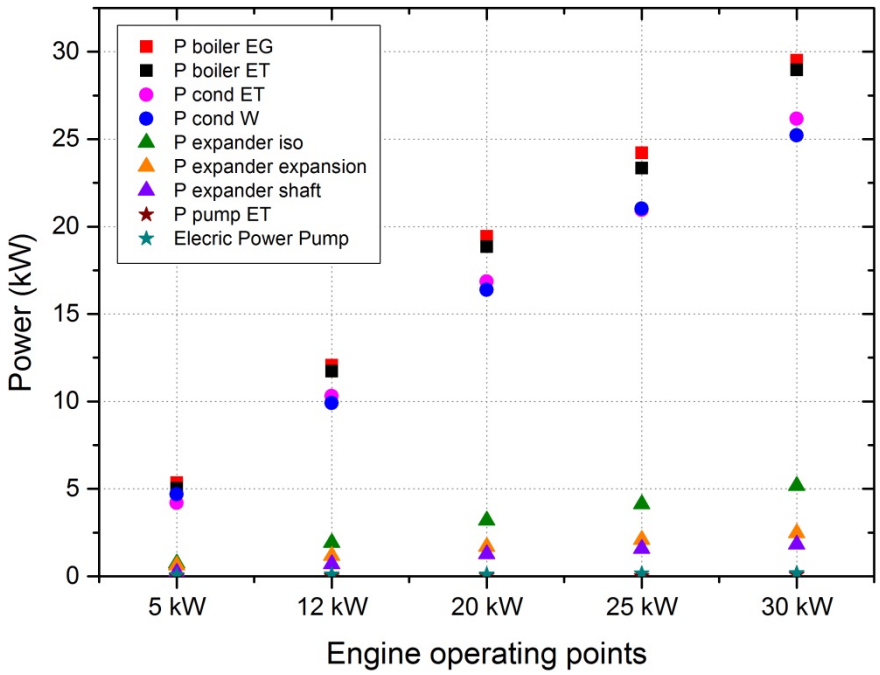

Fig. 6. Power balances operating points

The energy balance is reflected in Fig. 6. Under the five operating points, energy balances in the analyzed elements fit quite well and the maximum deviation is 0.91 kW at the point of 30 kW, which represents a relative deviation of 3%. Differences could be explained due to inaccuracies in specific calorific power estimations in both the water and the exhaust gases and in the uncertainties of temperature measurement. On the contrary, although pipes are insulated, heat

losses to the environment could appear. In order to estimate the global balance of the cycle the sum of $E_{boiler\ ET}$ and $E_{pump\ ET}$ has been compared with the sum of $E_{cond\ ET}$ and $E_{exp\ ET}$ and the maximum deviation is 0.405 kW at 30 kW point.

The energy balances for 30 kW are gathered in Fig. 7 using a Sankey Diagram [54]. The Sankey Diagram is divided in two parts: The first one corresponds to the ICE energy balance, which results in 32% of mechanical power, 26% of exhaust gases energy and 42% in cooling water energy. From exhaust gases, the WHRS could be splitted in four parts: The first one corresponds to the total power absorbed by the boiler from external sources (Exhaust gases and pump). The second part corresponds to the net energy available in the cycle taking into account efficiency of both the boiler and the pump. The third part corresponds with the maximum amount of energy (Isentropic power) that could be recovered with the expander. The last part shows the shaft power delivered by the expander, which results in a global expander efficiency of approximately 38%. The remainder power is released as heat to the environment through the exhaust line, the pump, the evaporator, internal irreversibilities in the expander and the condenser.

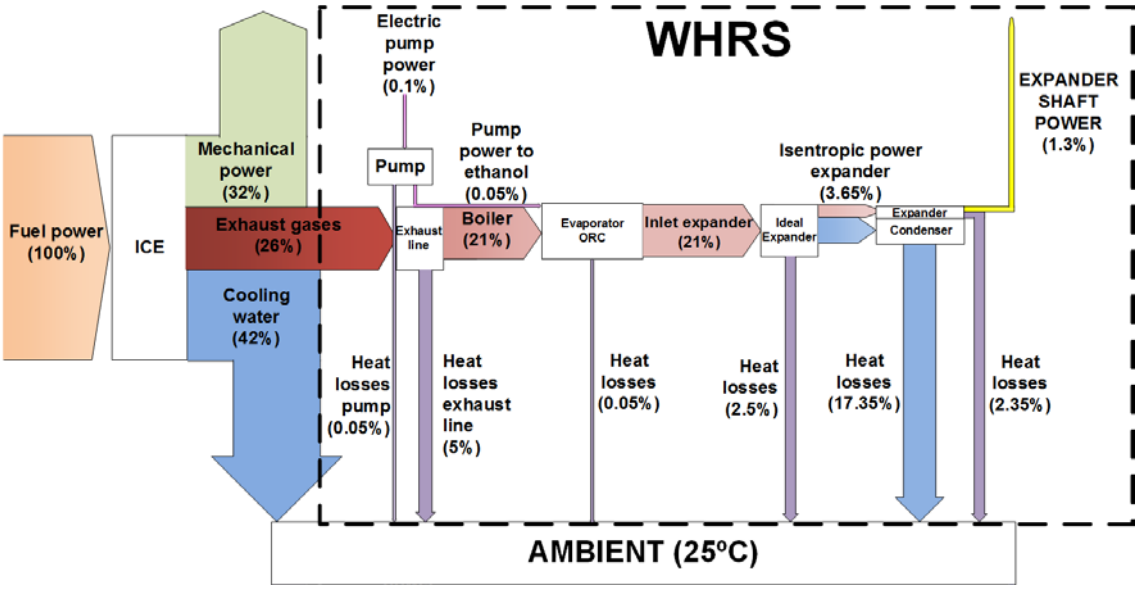

Fig. 7. Sankey diagram of 30 kW

Similar tendencies were appreciated in the Sankey diagrams of the remaining boiler powers, but 30 kW is represented due to its greater recovery potential and its lower level of uncertainty in measurements.

4. Cycle efficiencies

4.1. Engine-ORC efficiencies

Efficiency of the Gasoline engine (η_{GE}) is the ratio of the total engine mechanical power and the calorific fuel power:

$$\eta_{GE} = \frac{P_{GE}}{Q_{fuel}} \tag{15}$$

Where P_{GE} is the mechanical power of the gasoline engine (calculated using the engine torque, τ_{engine} and the engine speed,N_{engine}) and Q_{fuel} is total power obtained from the calorific value of the injected fuel.

Efficiency of the ORC-GE (η_{ORC-GE}) is the ratio of the difference between mechanical expansion power (P_{Exp_shaft}) and the electric power consumed by the

pump (Pe_{Pump_ET}) to the total power obtained from the calorific value of the injected fuel (Q_{fuel}). It is defined in Eq. 16.

$$\eta_{ORC-GE} = \frac{P_{Exp\_shaft} - Pe_{Pump\_ET}}{Q_{fuel}} \quad (16)$$

Efficiency of the ORC-GE$_{mec}$ is the ratio of the difference between mechanical expansion power (P_{Exp_shaft}) and the electric power consumed by the pump (Pe_{Pump_ET}) to the mechanical power of the engine (P_{GE}).

$$\eta_{ORC-GE_{mec}} = \frac{P_{Exp\_shaft} - Pe_{Pump\_ET}}{P_{GE}} \quad (17)$$

Where P_{GE} is the mechanical power of the gasoline engine defined in Eq. 15. The available power of the exhaust gases can be expressed as Eq. 18:

$$\eta_{EG} = \frac{P_{Boil\_EG}}{Q_{fuel}} \quad (18)$$

Where P_{Boil_EG} is the available power between inlet and outlet conditions of exhaust gases and Q_{fuel} is the total power obtained from the calorific value of the injected fuel.

4.2. Rankine and Carnot efficiencies

Three global efficiencies are taken into account: the Carnot efficiency (Eq. 19), the ideal Rankine efficiency (Eq. 20) and real Rankine efficiency (Eq. 21).

$$\eta_{Carnot} = 1 - \frac{T_l}{T_u} \quad (19)$$

Where T_l and T_u are respectively, the average lower temperature and the average upper temperature of the cycle process.

$$\eta_{Rankine_{ideal}} = \frac{P_{Exp\_isentropic} - P_{Pump\_ET}}{P_{Boil\_ET}} \quad (20)$$

Where $P_{Exp\_isentropic}$ is the expansion power delivered by the expander considering an isentropic process, P_{Pump_ET} is the power increase between inlet and outlet conditions of ethanol in the pump and P_{Boil_ET} is the power increase between inlet and outlet conditions of ethanol in the boiler.

$$\eta_{Rankine_{real}} = \frac{P_{Exp\_shaft} - Pe_{Pump\_ET}}{P_{Boil\_EG}} \quad (21)$$

Where P_{Exp_shaft} is the shaft power delivered by the expander, Pe_{Pump_ET} is the electric power required to pressurize the ethanol in the pump and P_{Boil_EG} is the power increase between inlet and outlet conditions of exhaust gases in the boiler. In later versions of this ORC cycle prototype, the ethanol pump will be coupled directly to the IC engine shaft, whereby the power consumed by the pump could be reduced.

4.3. Expander efficiencies

Two performance indexes are considered: The expander isentropic efficiency, $\eta_{\exp\_is}$, and the volumetric efficiency, $\eta_{\exp\_vol}$.

$$\eta_{\exp\_is} = \frac{P_{Exp\_shaft}}{P_{Exp\_isentropic}} \quad (22)$$

$$\eta_{\exp\_vol} = \frac{\dot{m}_{ET}}{\rho_{ET} * N_{exp} * D} \quad (23)$$

Where P_{Exp_shaft} and $P_{Exp\_isentropic}$ are the mechanical power of the expander shaft and the isentropic expansion power respectively, $\dot{m}_{ET}$, ρ_{ET} are the mass flow through the expander and the density of the ethanol at the inlet of the expander. Moreover, N_{exp} and D are the expander speed and the volume displaced by the expander, which is 79.954 cm^3.

4.4. Experimental results (Cycle efficiencies)

A summary of the engine ORC efficiencies obtained for each operating point is presented in Table 6. These values are plotted in Fig. 8.

Table 6. Engine ORC efficiencies

Engine operating points (kW)	η_{GE} (%=)	$\eta_{ORC\text{-}GE\_mec}$ (%)	$\eta_{ORC\text{-}GE}$ (%)	η_{EG} (%)
5	30.56	1.19	0.36	13.06
12	31.24	2.79	0.87	17.22
20	32.07	3.61	1.16	19.41
25	32.30	3.70	1.19	20.29
30	31.86	3.65	1.16	20.96

Fig. 8 shows engine ORC efficiencies for each operating point of the engine. The mechanical efficiency of the engine (η_{GE}) remains almost constant for all operating points, slightly increasing with operating points up to 25 kW and decreasing gradually with the highest engine operating point due to higher mechanical losses and engine optimization characteristics. As regards recovery potential from exhaust gases (η_{EG}), it increases significantly with the engine operating point. The reason is that while the engine operating point keeps rising,

fuel injected increases as well and consequently, large quantity of energy is available in the exhaust gases. Although the amount of fuel entered to the engine is high, this is lower than the power of the exhaust gases. This efficiency (η_{EG}) represents the maximum energy that could be absorbed from the exhaust gases, which varies from 13.06% at lower loads and 20.96% at higher loads. Nevertheless, in the ORC there are several irreversibilities, such as friction losses, non isentropic processes and heat losses to the environment. Thus, the maximum efficiency that could be reached in the cycle decreases greatly regarding the exhaust gases efficiency (η_{EG}). Generally speaking, similar tendencies are shown in the mechanical efficiency of the engine (η_{GE}) and the efficiencies concerning fuel input power (η_{ORC-GE}) and mechanical engine power ($\eta_{ORC-GE_{mec}}$). They both follow a similar tendency, reaching during the test with our bill of material based on prototype and not optimized, a maximum value of 1.19% and 3.7% respectively with 25 kW. Although higher recovery potential in the exhaust gases (η_{EG}) is observed with increasing operating points, different trends are shown in η_{ORC-GE} and $\eta_{ORC-GE_{mec}}$. In both indexes the maximum value is obtained at 25 kW due to the fact that, as shown in Table 4, lower expander speeds are required at 25 kW comparing to 20 kW and 30 kW. Therefore, mechanical losses are minimized at this point.

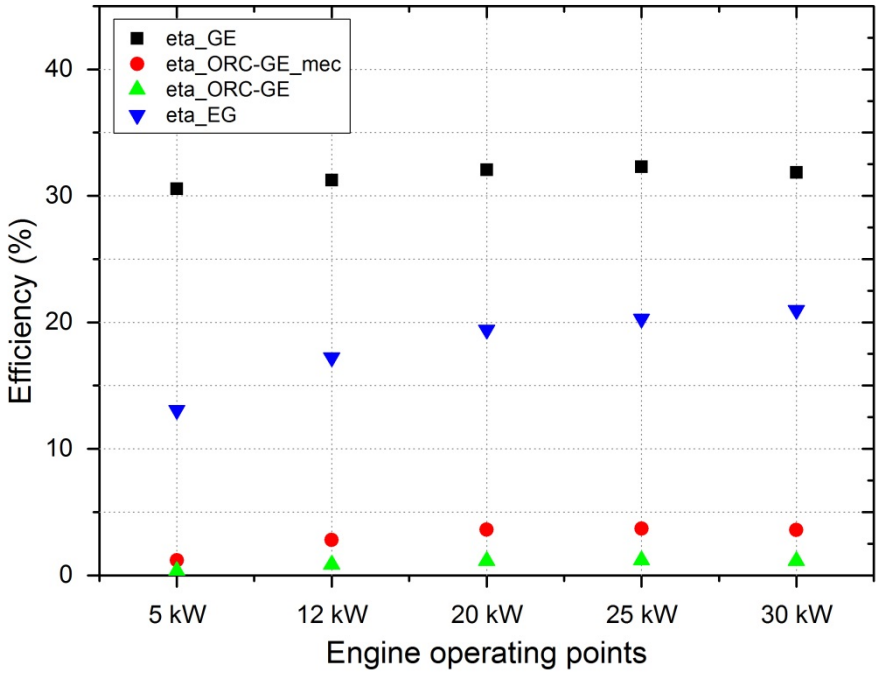

Fig. 8. Engine ORC efficiencies for operating points

A summary of the Rankine and Carnot efficiencies obtained for each operating point is presented in Table 7. Under these five conditions, the Carnot efficiency, η_{Carnot}, decreases when the operating point increases, whereas, the efficiency of the Rankine cycle, $\eta_{Rankine_{ideal}}$, increases constantly with the increase of the operating point. As regards $\eta_{Rankine_{real}}$, it can be seen that it reaches its maximum value at 20 kW.

Table 7. Rankine and Carnot efficiencies

Engine operating Points (kW)	Carnot efficiency (%)	Rankine ideal efficiency (%)	Rankine Actual efficiency (%)
5	80.78	14.60	2.79
12	79.31	16.37	5.07
20	78.63	17.26	5.97
25	78.35	17.47	5.89
30	76.81	17.62	5.55

The Carnot efficiency is a theoretical efficiency estimation considering an ideal approach based on a cycle process made up by isentropic compression and expansion and isochoric supply and heat transfer. The evolution of Carnot efficiency shows a flat trend in all operating points. It can be seen that, it decreases slightly with the increasing operating point due to the increase in the lower level of temperature in the cycle for higher operating points. It reaches its maximum value of 80.78% at 5 kW operating point. The Rankine ideal efficiency computes the ideal amount of energy available in the cycle, so that, it increases as the power of exhaust gases is magnified because higher quantity of energy is available at the exhaust gases and thus, the isentropic power of the expander is higher. Its reaches its maximum value of 17.62% at 30 kW operating point. On the other hand, Rankine real efficiency takes into account irreversibilities of the expander, thus, its maximum is not obtained in the maximum boiler power, but at 20 kW with a value of 5.97%. Contrary to Rankine ideal efficiency, which keeps rising with increasing operating points, the Rankine real efficiency reach a peak

at 20 kW due to, as it can be seen in Table 4, optimal expander conditions are fixed, using a expander speed of 3511 rpm and an expansion ratio of 9.2. These conditions seem to be the best ones where the working fluid expansion fits better with volumetric expansion ratio of this swash-plate expander. To sum up, although there is a great recovery potential in the exhaust gases of ICE, the influence of adding an expansion machine is clearly visible comparing Carnot efficiency (approximately 80%) to ideal Rankine efficiency (approximately 17%), which takes into account an isentropic expansion machine, and to real Rankine efficiency (approximately 6%), which takes into account irreversibilities of the process, including heat losses to the environment and pressure drop.

5. Sensitivity analysis

In this section 28 steady-state points were analyzed to evaluate cycle and expander efficiencies under different expander parameters, i.e. expansion ratio, expander speed and outlet pressure of the expander. For each boiler power (5, 12, 20, and 25 kW) two different outlet expander pressures were tested. Increasing operating points with higher mass flows were tested by changing pump speed. The lower pressure limit was imposed due to limitations of cooling temperature in the vehicle cooling system. It was controlled by the balloon pressure of the expander vessel. Tests were performed changing expander speed from 1000 to 5000 rpm. High pressure was imposed by the expander speed regulation. Temperature at the inlet of the expander is fixed around 225°C in order to maintain a certain degree of superheating.

5.1. Engine ORC efficiencies

Fig. 9 shows the variation of shaft power with expansion ratio for different boiler power. The expander shaft power appears to increase at first and then reaches

a maximum of 0.213 kW, 0.677 kW, 1.171 kW and 1.57 kW at 5 kW, 12 kW, 20 kW and 25 kW respectively. Sequentially, the power delivered by the expander decreases with increasing expansion ratios (above the value of 6.4 with 5 kW, 7.6 with 12 kW and 9.4 with 20 and 25 kW). When the expansion ratio is lower than the optimum one, leakages effects and over-expansion losses appear, whereas, when the expansion ratio is above the optimum point, under expansion effects are shown. In both cases, the expander shaft power is reduced. The optimum value is performed when the working fluid expansion ratio matches with the built-in volumetric expansion ratio, which for this particular expander corresponds to a value of 7.633. The same tendency could be noticed in every boiler power. The maximum shaft power is gained under the boiler operating point of 25 kW (30 kW studies were not performed) and running expander speed at 3000 rpm, with a shaft power value of 1.57 kW. Variation of ORC-GE$_{_mec}$ efficiencies with expansion ratio are gathered in Fig. 10. The reduction of engine operating load from operating point 5 to 1 results in a η_{ORC-GE_mec} drop from 3.7% to 0.5%. Similar tendencies as Fig. 9 are shown in Fig. 10. It reveals that the maximum η_{ORC-GE_mec} of each boiler power is obtained by increasing expansion ratios until a maximum value, i.e. 1.19% in 5kW, 2.59% in 12kW, 3.15% in 20kW and 3.7% in 25kW. It can be concluded that under high engine operating points a potential of improvement in engine mechanical efficiency could be made, by increasing it upon conventional engine at least in a 3.7%. Similar tendencies in η_{ORC-GE_mec} and the power delivered by the expander could be seen comparing Fig. 11 and Fig. 12, except for curves with 20 kW and 25 kW, which seems to collapse in a single curve at low expansion ratios. Uncertainty propagation of the measured values (P_{Exp_shaft},$\eta_{ORC-GE_{mec}}$, $\eta_{Rankine_{ideal}}$ and $\eta_{Rankine_{real}}$) have been

calculated as a function of one or more measured variables upon which they depend. This Method is described in NIST Technical Note 1297 [55]. They are shown from Fig. 9 to Fig. 12.

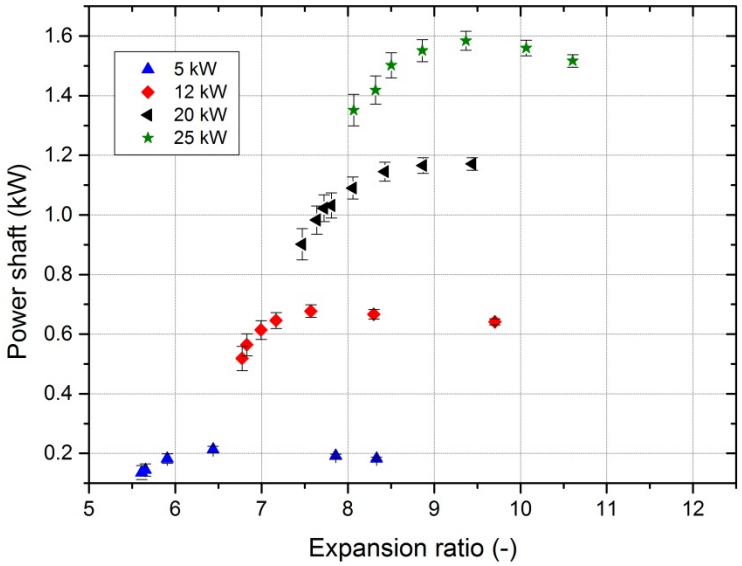

Fig. 9. Variation of power shaft with expansion ratio for different boiler power

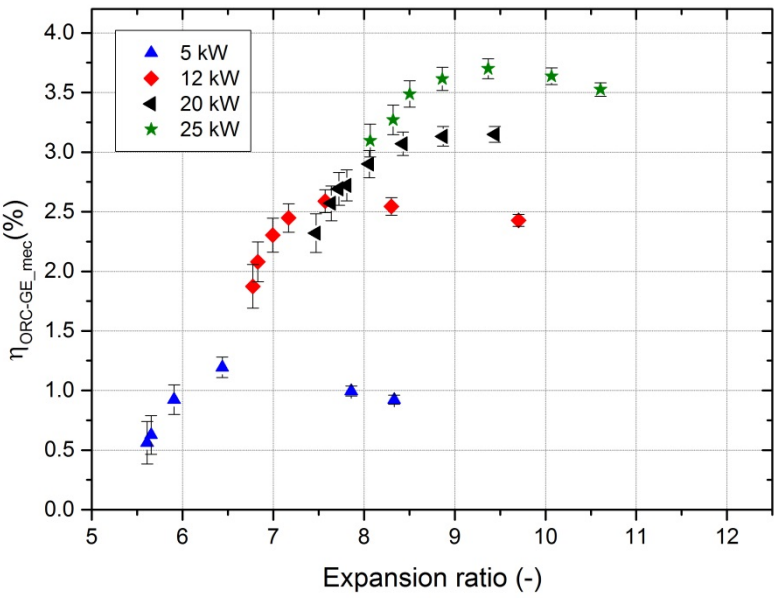

Fig. 10. Variation of η_{ORC-GE_mec} with expansion ratio

5.2. Rankine efficiencies

Fig. 11 and Fig. 12 present ideal and real Rankine efficiencies respectively.

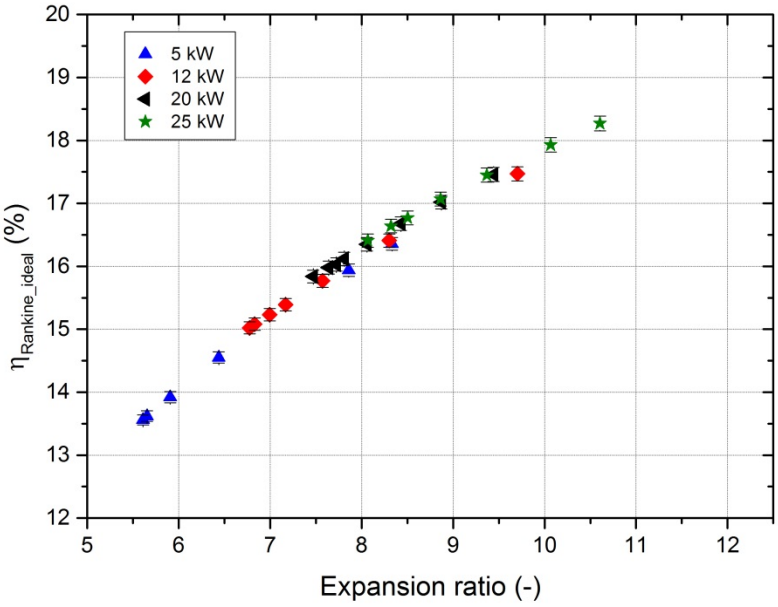

Fig. 11. Variation of Rankine ideal efficiency with expansion ratio

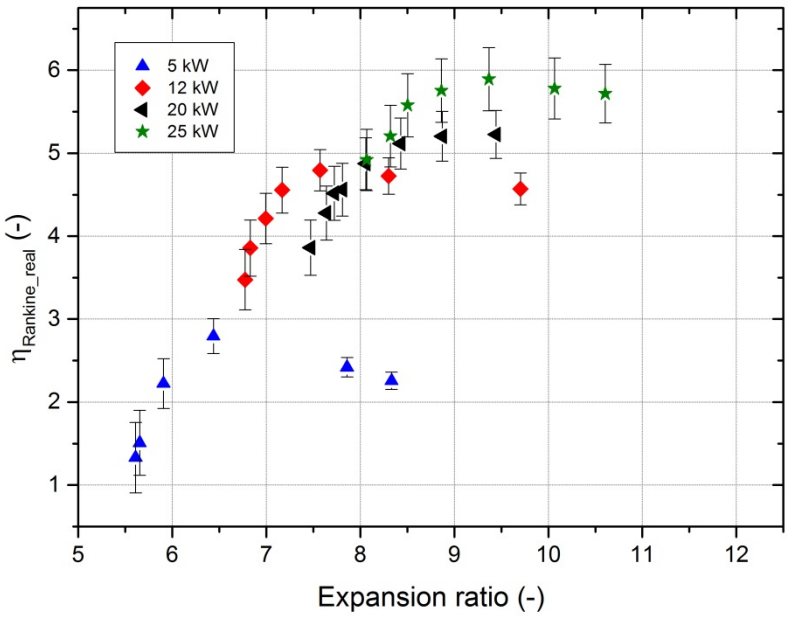

Fig. 12. Variation of Rankine real efficiency with expansion ratio

Rankine ideal efficiency is calculated taking into account isentropic power and heat absorbed by the ethanol. As shown in Fig. 11, ideal Rankine efficiency in the system increases with the expansion ratio (from 5.5 to 11), following a similar tendency in every boiler power. Generally speaking, increments in expansion ratios involved increments in the differences of high and low temperatures of the cycle and greater isentropic power delivered by the expansion process. Thus, for each boiler power, as the expansion ratio is increased, the isentropic power is enhanced while the rest of the parameters that affect Rankine ideal efficiency, P_{Boiler_ET} and P_{Pump_ET}, have not significantly changed. Rankine ideal efficiency increases with expansion ratio because it is considered inlet (enthalpy) and outlet (pressure) conditions to calculate isentropic power. Ideal Rankine efficiencies varies from 14% to 19%. Similar values are reported in literature [27].

In Fig. 12 Rankine real efficiency is reported as a function of the expansion ratio, for different boiler power. It shows a global tendency similar to Fig. 11. As stated before, the maximum Rankine real efficiency for each boiler power is obtained increasing expansion ratio with peaks at 6.4, 7.6 and 9.4 at 5, 12 and 20/25 kW respectively. Differences between ideal and real Rankine efficiency exist due to irreversibilities of the expansion machine. Therefore, although a potential Rankine efficiency of 19% is obtained at high operating points using an ideal isentropic machine, indeed, a maximum real Rankine efficiency of 6% is achieved considering heat losses to the environment and real expansion and compression processes.

5.3. Expander efficiencies

Volumetric efficiency could be used to compute engine performance in terms of movement of charge into and out of the cylinders. It is used to evaluate the intake

process and to compare different intake technologies. Volumetric efficiency as a function of expander speed and expansion ratio is plotted in Fig. 13 for the same points of previous figures.

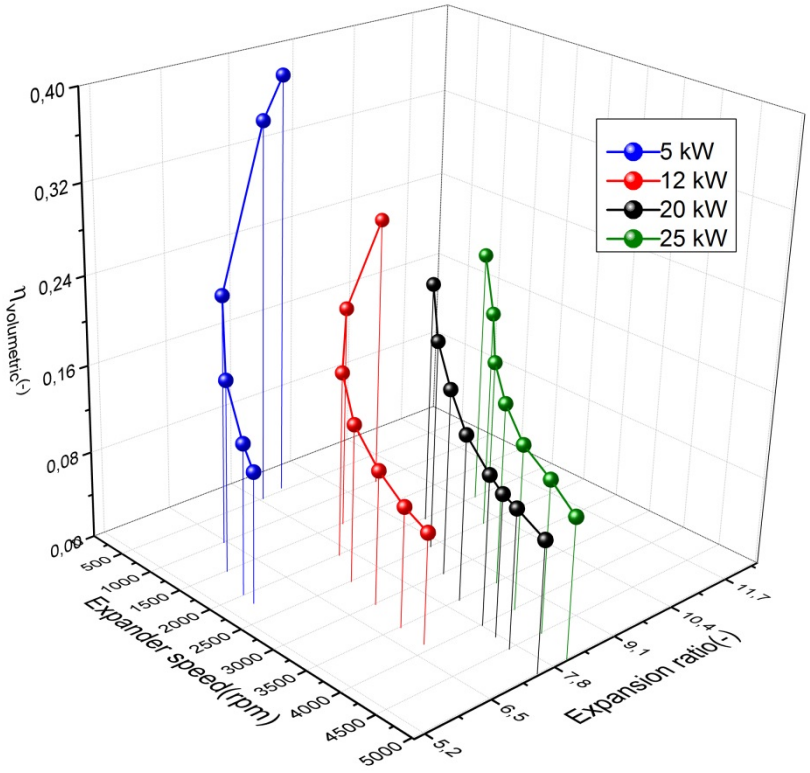

Fig. 13. Variation of volumetric efficiency with expansion ratio and expander speed

As shown in Fig. 13, volumetric efficiency is a monotonically increasing function of expander speed and expansion ratio. In these points, a maximum value of 38.5% is reached at 5 kW. As the expander speed rise up, less time is available to introduce ethanol in the cylinders, which results in lower volumetric efficiencies by increasing expander speeds, obtaining a lower value of 5% at the highest expander speed (5500 rpm). In terms of expansion ratio, the higher it is, the better volumetric efficiency is achieved because higher expansion rates involved higher inlet pressures, which will help the ethanol to enter the cylinders.

The second important performance parameter of the expander is the isentropic efficiency calculated by Eq. 22. As it is indicated in Fig. 14, the isentropic efficiency reaches a maximum, which is different depending on the boiler power and the outlet pressure at the expander. Thus, the pressure ratio that maximizes the isentropic efficiency is not constant for all rotational speeds. Leakages, friction losses, pressure drop at the inlet and outlet processes and heat losses [10] could influence this peak of isentropic efficiency. The maximum value, 38.2%, is obtained with an expander speed of 3021 rpm and an expansion ratio of 9.4 at the point of 25 kW. For each boiler power it could be seen that lower expander speeds and higher pressure ratios lead to an expander performance drop due to the effect of leakages, whereas higher expander speed and lower pressure ratios lead to a sharply reduction in the expander isentropic efficiency due to the effect of mechanical losses and intake pressure drop. Therefore, there is an optimal expander speed and expansion ratio for each boiler power and outlet pressure. Peaks of isentropic efficiency corresponds to 28.8% (5 kW), 36.4% (12 kW), 34.6% (20 kW) and 38.3% (25 kW).

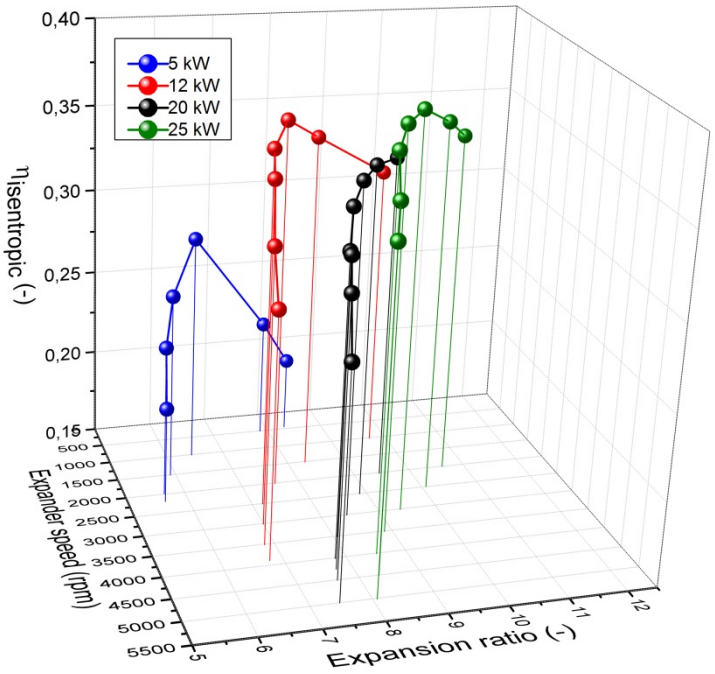

Fig. 14. Variation of isentropic efficiency with expansion ratio and expander speed

To sum up, the pressure ratio that optimizes the isentropic efficiency is not constant for all boiler powers (Fig. 14). The maximum value is fixed by the built-in volumetric expansion ratio, which for this particular expander corresponds to a value of 7.633. However, it only matches this value at low boiler powers. With low boiler power (5 kW), the ethanol mass flow pumped through the installation is lower than the one circulating in 25 kW. If the ethanol mass flow is low, lower expander speeds are required to fill in the cylinders and therefore, lower inlet pressures (and expansion ratios) are obtained. This behavior can be observed in Fig. 13, getting higher volumetric efficiencies with lower boiler power and lower expander speeds. Therefore, higher boiler powers implies higher ethanol mass flows and higher expander speeds. Consequently, higher pressure ratios are required during the intake and exhaust processes of the expander in order to enter the ethanol into the cylinders. Because of this, the optimal pressure ratio

between the inlet and outlet of the expander increases as the power available to the expander increases.

Volumetric and isentropic efficiencies have been correlated using points discussed in previous chapters in order to model the entire ORC system. It will allow developing an indispensable tool to simulate steady and transient points and for being able to identify the influence of the operating parameters and predict the behavior of the system at critical operating points.

6. Conclusions

This paper describes and analyzes an experimental installation of an ORC system installed in a turbocharged 2.0 liter gasoline engine to recover waste heat in exhaust gases. Energy balances for different boiler powers between 5 kW and 30 kW are presented, showing substantial differences in terms of mechanical power delivered by the expander, which results in a value of 0.21 kW and 1.83 kW respectively. The evolution of several efficiency parameters have been reviewed by means of changing the main parameters affecting the ORC cycle, which are the expansion ratio, the expander speed and the outlet pressure of the expander. The following results have been obtained with available bill of material based on prototypes

1. A potential of increasing ICE mechanical efficiency up to 3.7% could be reached at points of high load (25 kW) installing an ORC in a conventional turbocharged gasoline engine.
2. A maximum Carnot efficiency, Rankine ideal efficiency and Rankine real efficiency values of 79%, 19% and 6% could be obtained using a swash-

plate expander to recover energy from exhaust gases. Similar values are achieved in the scientific literature.

3. Isentropic and volumetric efficiency were used to evaluate performance of the swash-plate expander. Maximum values of 38.5% and 38.2% were obtained respectively.

Future work will focus on the development of an accurate model of both the swash-plate expander and the ORC system in order to simulate steady and transient points and to be able to identify the influence of the operating parameters and predict the behavior of the system at critical operating points. Another target is to specify new bill of material and estimate how the system could be improved. Considering the capacity of improvement in expander efficiencies and thermal insulation of different elements of the facility, it can be concluded that the ethanol ORC provides an interesting field of study to consider in the coming years.

7. Acknowledgements

This work is part of a research project called “Evaluation of bottoming cycles in IC engines to recover waste heat energies” funded by a National Project of the Spanish Government with reference TRA2013-46408-R.

REFERENCES

[1] J. Rodrigue, C. Comtois, and B. Slack, *The Geography of Transport Systems*. 2006, p. 297.

[2] S. A. H. T. A, “Factors That Will Influence Oil and Gas Supply and Demand in the 21st Century,” *MRS Bull.*, vol. 33, pp. 317–323, 2010.

[3] R. El Chammas and D. Clodic, “Combined Cycle for Hybrid Vehicles,” *SAE Int.*, vol. 1, p. 10, 2012.

[4] T. A. Horst, W. Tegethoff, P. Eilts, and J. Koehler, “Prediction of dynamic Rankine Cycle waste heat recovery performance and fuel saving potential in passenger car applications considering interactions with vehicles’ energy management,” *Energy Convers. Manag.*, vol. 78, pp. 438–451, Feb. 2014.

[5] R. Daccord, A. Darmedru, and J. Melis, “Oil-free axial piston expander for waste heat recovery,” *SAE Int.*, vol. 1, pp. 1–12, Apr. 2014.

[6] Roland Berger, “Trends in ICE-Technologies Besides Electrification , improvements in conventional powertrain technologies will play a major role looking forward,” in *Automotive megatrends*, 2013, pp. 1–13.

[7] N. Espinosa, L. Tilman, V. Lemort, S. Quoilin, and B. Lombard, “Rankine cycle for waste heat recovery on commercial trucks: approach, constraints and modelling,” *Diesel Int. Conf. Exhib.*, vol. 1, pp. 1–10, May 2010.

[8] I. Vaja and A. Gambarotta, “Internal Combustion Engine (ICE) bottoming with Organic Rankine Cycles (ORCs),” *Energy*, vol. 35, no. 2, pp. 1084–1093, Feb. 2010.

[9] T. Wang, Y. Zhang, Z. Peng, and G. Shu, “A review of researches on thermal exhaust heat recovery with Rankine cycle,” *Renew. Sustain. Energy Rev.*, vol. 15, no. 6, pp. 2862–2871, Aug. 2011.

[10] S. Declaye, S. Quoilin, L. Guillaume, and V. Lemort, “Experimental study on an open-drive scroll expander integrated into an ORC (Organic Rankine Cycle) system with R245fa as working fluid,” *Energy*, vol. 55, pp. 173–183, Jun. 2013.

[11] V. Lemort, S. Quoilin, C. Cuevas, and J. Lebrun, “Testing and modeling a scroll expander integrated into an Organic Rankine Cycle,” *Appl. Therm. Eng.*, vol. 29, no. 14–15, pp. 3094–3102, Oct. 2009.

[12] A. Legros, L. Guillaume, V. Lemort, M. Diny, I. Bell, and S. Quoilin, “Investigation on a scroll expander for waste heat recovery on internal

combustion engines," *Int. Conf. compressors their Syst.*, vol. 1, p. 10, 2013.

[13] S. Quoilin, V. Lemort, and J. Lebrun, "Experimental study and modeling of an Organic Rankine Cycle using scroll expander," *Appl. Energy*, vol. 87, no. 4, pp. 1260–1268, Apr. 2010.

[14] M. Tahir, N. Yamada, and T. Hoshino, "Efficiency of Compact Organic Rankine Cycle System with Rotary-Vane-Type Expander for Low-Temperature Waste Heat Recovery," in *World Academy of Science, Engineering and Technology 37*, 2010, pp. 906–911.

[15] B. Yang, X. Peng, Z. He, B. Guo, and Z. Xing, "Experimental investigation on the internal working process of a CO2 rotary vane expander," *Appl. Therm. Eng.*, vol. 29, no. 11–12, pp. 2289–2296, Aug. 2009.

[16] R. Cipollone, G. Bianchi, D. Di Battista, G. Contaldi, and S. Murgia, "Mechanical Energy Recovery from Low Grade Thermal Energy Sources," *Energy Procedia*, vol. 45, pp. 121–130, 2014.

[17] A. Della Torre, G. Montenegro, M. Fiocco, and A. Onorati, "Evaluating the Performance of a Rotary Vane Expander for Small Scale Organic Rankine Cycles using CFD tools," in *68º Conference of the Italian Thermal Machines Engineering Association*, 2014, pp. 1136–1145.

[18] Y. Glavatskaya, P. Podevin, V. Lemort, O. Shonda, and G. Descombes, "Reciprocating Expander for an Exhaust Heat Recovery Rankine Cycle for a Passenger Car Application," *Energies*, vol. 5, no. 12, pp. 1751–1765, Jun. 2012.

[19] W. Yagoub, P. Doherty, and S. B. Riffat, "Solar energy-gas driven micro-CHP system for an office building," *Appl. Therm. Eng.*, vol. 26, no. 14–15, pp. 1604–1610, Oct. 2006.

[20] T. Yamamoto, "Design and testing of the Organic Rankine Cycle," *Energy*, vol. 26, pp. 239–251, 2001.

[21] D. Seher, T. Lengenfelder, J. Gerhardt, N. Eisenmenger, M. Hackner, and I. Krinn, "Waste Heat Recovery for Commercial Vehicles with a Rankine Process," in *21 st Aachen Colloquium Automobile and Engine Technology*, 2012, pp. 1–15.

[22] H. J. Kim, J. M. Ahn, I. Park, and P. C. Rha, "Scroll expander for power generation from a low-grade steam source," *Proc. Inst. Mech. Eng. Part A J. Power Energy*, vol. 221, no. 5, pp. 705–711, Jan. 2007.

[23] R. B. Peterson, H. Wang, and T. Herron, "Performance of a small-scale regenerative Rankine power cycle employing a scroll expander," *Proc. Inst. Mech. Eng. Part A J. Power Energy*, vol. 222, no. 3, pp. 271–282, May 2008.

[24] D. Manolakos, G. Kosmadakis, S. Kyritsis, and G. Papadakis, “Identification of behaviour and evaluation of performance of small scale, low-temperature Organic Rankine Cycle system coupled with a RO desalination unit,” *Energy*, vol. 34, no. 6, pp. 767–774, Jun. 2009.

[25] V. Lemort, S. Declaye, and S. Quoilin, “Experimental characterization of a hermetic scroll expander for use in a micro-scale Rankine cycle,” *Proc. Inst. Mech. Eng. Part A J. Power Energy*, vol. 226, no. 1, pp. 126–136, Nov. 2011.

[26] R. Bracco, S. Clemente, D. Micheli, and M. Reini, “Experimental tests and modelization of a domestic-scale ORC (Organic Rankine Cycle),” *Energy*, vol. 58, pp. 107–116, Sep. 2013.

[27] T. Endo, S. Kawajiri, Y. Kojima, K. Takahashi, T. Baba, S. Ibaraki, T. Takahashi, and M. Shinohara, “Study on Maximizing Exergy in Automotive Engines,” *SAE Int.*, vol. 1, pp. 1–12, 2007.

[28] J. Bao and L. Zhao, “A review of working fluid and expander selections for organic Rankine cycle,” *Renew. Sustain. Energy Rev.*, vol. 24, pp. 325–342, Aug. 2013.

[29] F. Mechanics, S. Quoilin, and C. Sart-tilman, “Expansion Machine and Fluid Selection for the Organic Rankine Cycle,” in *7th International Conference on Heat Transfer, Fluid Mechanics and Thermodynamics*, 2010, no. July, pp. 1–7.

[30] G. Latz, S. Andersson, and K. Munch, “Selecting an Expansion Machine for Vehicle Waste-Heat Recovery Systems Based on the Rankine Cycle,” *SAE Int.*, vol. 1, pp. 1–15, Apr. 2013.

[31] J. B. Heywood, *Internal combustion engine fundamentals*. 1988, pp. 1–930.

[32] A. Duparchy, P. Leduc, G. Bourhis, and C. Ternel, “Heat Recovery for next Generation of Hybrid Vehicles : Simulation and Design of a Rankine Cycle System,” *World Electr. Veh. J. Vol.3*, vol. 3, pp. 1–17, 2009.

[33] H. Teng, G. Regner, and C. Cowland, “Waste Heat Recovery of Heavy-Duty Diesel Engines by Organic Rankine Cycle Part I: Hybrid Energy System of Diesel and Rankine Engines,” *SAE Int.*, vol. 1, no. 724, pp. 1–13, Apr. 2007.

[34] V. Macián, J. R. Serrano, V. Dolz, and J. Sánchez, “Methodology to design a bottoming Rankine cycle, as a waste energy recovering system in vehicles. Study in a HDD engine,” *Appl. Energy*, vol. 104, pp. 758–771, Apr. 2013.

[35] V. Dolz, R. Novella, a. García, and J. Sánchez, “HD Diesel engine equipped with a bottoming Rankine cycle as a waste heat recovery

system. Part 1: Study and analysis of the waste heat energy," *Appl. Therm. Eng.*, vol. 36, pp. 269–278, Apr. 2012.

[36] R. Freymann, "The Turbosteamer : A System Introducing the Principle of Cogeneration in," *MTZ*, vol. 69, no. 5, pp. 20–27, 2008.

[37] H. Teng, J. Klaver, T. Park, G. L. Hunter, and B. van der Velde, "A Rankine Cycle System for Recovering Waste Heat from HD Diesel Engines - WHR System Development," *SAE Int.*, vol. 1, pp. 1–11, Apr. 2011.

[38] A. Boretti, "Recovery of exhaust and coolant heat with R245fa organic Rankine cycles in a hybrid passenger car with a naturally aspirated gasoline engine," *Appl. Therm. Eng.*, vol. 36, pp. 73–77, Apr. 2012.

[39] S. Quoilin, M. Van Den Broek, S. Declaye, P. Dewallef, and V. Lemort, "Techno-economic survey of Organic Rankine Cycle (ORC) systems," *Renew. Sustain. Energy Rev.*, vol. 22, pp. 168–186, Jun. 2013.

[40] G. Shu, L. Liu, H. Tian, H. Wei, and G. Yu, "Parametric and working fluid analysis of a dual-loop organic Rankine cycle (DORC) used in engine waste heat recovery," *Appl. Energy*, vol. 113, pp. 1188–1198, Jan. 2014.

[41] H. Teng, G. Regner, and A. V. L. P. Engineering, "Improving Fuel Economy for HD Diesel Engines with WHR Rankine Cycle Driven by EGR Cooler Heat Rejection," *SAE Int.*, vol. 1, pp. 1–11, Oct. 2009.

[42] D. Ziviani and A. Beyene, "Advances and challenges in ORC systems modeling for low grade thermal energy recovery," *Appl. Energy*, vol. 121, pp. 79–95, 2014.

[43] Y. Dai, J. Wang, and L. Gao, "Parametric optimization and comparative study of organic Rankine cycle (ORC) for low grade waste heat recovery," *Energy Convers. Manag.*, vol. 50, no. 3, pp. 576–582, Mar. 2009.

[44] B. Saleh, G. Koglbauer, M. Wendland, and J. Fischer, "Working fluids for low-temperature organic Rankine cycles," *Energy*, vol. 32, no. 7, pp. 1210–1221, Jul. 2007.

[45] V. Maizza and A. Maizza, "Unconventional working fluids in organic Rankine-cycles for waste energy recovery systems," *Appl. Therm. Eng.*, vol. 21, pp. 381–390, 2001.

[46] H. Tian, G. Shu, H. Wei, X. Liang, and L. Liu, "Fluids and parameters optimization for the organic Rankine cycles (ORCs) used in exhaust heat recovery of Internal Combustion Engine (ICE)," *Energy*, vol. 47, no. 1, pp. 125–136, Nov. 2012.

[47] Z. Q. Wang, N. J. Zhou, J. Guo, and X. Y. Wang, “Fluid selection and parametric optimization of organic Rankine cycle using low temperature waste heat,” *Energy*, vol. 40, no. 1, pp. 107–115, Apr. 2012.

[48] D. Wei, X. Lu, Z. Lu, and J. Gu, “Performance analysis and optimization of organic Rankine cycle (ORC) for waste heat recovery,” *Energy Convers. Manag.*, vol. 48, no. 4, pp. 1113–1119, Apr. 2007.

[49] J. Zhang, H. Zhang, K. Yang, F. Yang, Z. Wang, G. Zhao, H. Liu, E. Wang, and B. Yao, “Performance analysis of regenerative organic Rankine cycle (RORC) using the pure working fluid and the zeotropic mixture over the whole operating range of a diesel engine,” *Energy Convers. Manag.*, vol. 84, pp. 282–294, Aug. 2014.

[50] T. Howell and J. Gibble, “Development of an ORC system to improve HD truck fuel efficiency,” in *Deer Conference*, 2011, vol. 1, pp. 1–21.

[51] M. J. Moran, H. N. Shapiro, D. D. Boettner, and M. Bailey, *Fundamentals of Engineering Thermodynamics*. John Wiley & Sons, 2010, p. 944.

[52] M. Lapuerta, O. Armas, and J. J. Herna, “Diagnosis of DI Diesel combustion from in-cylinder pressure signal by estimation of mean thermodynamic properties of the gas,” *Appl. Therm. Eng.*, vol. 19, pp. 513–529, 1999.

[53] “REFPROP Version 7,” *NIST Standard Reference Database 23*, 1998. [Online]. Available: http://web.mit.edu/ruddman/Public/Thermodynamics/REFPROP7doc1.pdf. [Accessed: 21-May-2014].

[54] K. Soundararajan, H. Kwee, and B. Su, “A Sankey Framework for Energy and Exergy Flows,” in *ICEST*, 2013, no. February, pp. 1–13.

[55] B. N. Taylor and C. E. K. Kuyatt, “Guidelines for Evaluating and Expressing the Uncertainty of NIST Measurement Results,” *NIST Tech. Note 1297*, vol. 1, p. 20, 1994.